Modelling the Ballistic Missile Problem with the State Transition Matrix: An Analysis of Trajectories including a Rotating Earth and Atmospheric Drag

Semester Report

Justin S. McFarland
Virginia Tech, Blacksburg, VA 24061

May 11, 2004

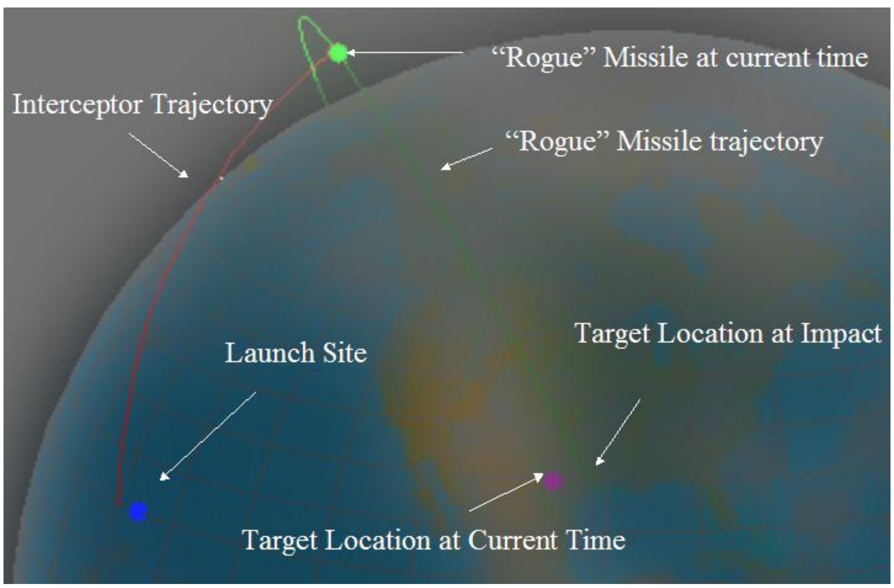

Abstract

The ballistic missile problem is a typical topic of discussion in introductory astromechanics courses when discussing Keplerian motion. This study revisits the introductory ballistic missile problem by modelling spherical Earth, Earth rotation, and addition of atmospheric drag. The scope of this exercise comprises launching from an initial set of coordinates in the form of latitude and longitude in the Earth frame to a desired target set of coordinates. As intuition suggests, resolving the target location increases in difficulty as the model complexity increases. Further, when a significant atmosphere is introduced, analytic solutions are no longer possible using traditional methods. Modern techniques are then explored using the state transition matrix, a sensitivity based tool, to correct the initial velocity guess in order to converge upon the desired target within a specified accuracy. An analytical solution of the two-body problem and a numerical approach are used to compute the state transition matrix. A comparison is made to determine the regions of convergence available to each of these techniques for an array of targets and various launch locations, in order to determine their usefulness in the form of number of iterations required to converge, trends if the solutions did not converge, and computational speed.

Nomenclature

a	Semimajor axis, km
f	True anomaly angle, rad
h	Altitude above surface, km
p	Semilatus rectum, km
$\boldsymbol{r}$	Trajectory radius, km
$\boldsymbol{V}$	Trajectory velocity, km/s
Δt	Time of flight, s
$\Delta \boldsymbol{V}$	Change in velocity, km/s
Λ	Atmosphere scale height, km
Φ_{12}	State transition matrix
β	Modified ballistic coefficient, kg/km^2
γ	Sidereal time, radians
$\delta \boldsymbol{r}_f$	Range error, km
$\delta \boldsymbol{v}$	Initial velocity correction, km/s
λ	Longitude, degrees
μ	Gravitational parameter, km^3/kg^2
ϕ	Latitude, degrees
ρ	Density, kg/km^3

Subscripts

x, y, z	Cartesian body axes, km
f	Final state
ref	Reference state
UT	Universal time
0	Initial state on surface

Superscripts

t	target

Constants

$\mu_{\text{Earth}} = 3.986 \times 10^5$ km^3/kg^2
$R_{\text{Earth}} = 6378$ km (mean Earth equatorial radius)
$\omega_{\text{Earth}} = 7.292115854670501 \times 10^{-5}$ rad/sec rotation rate with respect to inertial Earth

Contents

1 Introduction

The ballistic missile problem is typically represented in introductory astromechanics texts as a simplified planar two-body problem with a non-rotating Earth. From this information we can usually determine the range of a projectile, the initial flight path angle, the orbit eccentricity and semi-major axis, and its true anomaly angles at launch and impact. It is of interest to expand upon this basic model in order to add realism to the problem.

Applications desiring increased complexity include determining the initial launch vector direction and velocity requirements for a vehicle, simulation of the ground track of a hypersonic vehicle, orbit plane determination, analysis of energy required at various launch sites to reach different targets, and means to determine potential load factors, deceleration, and temperature gains of a body as it travels through the atmosphere. Additionally, interplanetary missions such as those to Mars and Venus may require high degree of landing accuracy when entering their respective atmospheres. Thus hyperbolic trajectories can also be utilized in order to resolve an appropriate, necessary velocity at a fixed point in space. More recently, missile defense applications require the modelling of the ballistic missile problem. Modelling the ballistic missile problem is the first part in series of requirements of modelling the system wide architecture of ballistic missile defense systems that also includes modelling the interceptor missile and tracking systems.

Modelling of the ballistic, unpowered free-flying point mass trajectory[1] requires high fidelity in order to make predictions and determine regions at risk. In order to make the necessary adjustments to the increased realism levels, the complexity of our system must be increased in order to account for the dynamics in a inertial, cartesian coordinate frame. To meet the need of this complexity, it is of further interest to utilize the power of modern computers in order to rapidly account for perturbations such as J_2 and atmospheric drag and the effects due to the rotation of the primary body.

Numerical integration techniques can be employed to account for effects such as those of a thrusting projectile through an atmosphere, the drag and lift on this body, and relevant effects of J_2 and other perturbations[2] of these problems. However, when perturbation methods are taken in to account, resolving the trajectory of the vehicle to arrive at a specified target is no longer a function of Keplerian motion. Modern techniques must be invoked in order to resolve the more complex dynamics of these systems. One such technique is the use of the state transition matrix (STM).

The state transition matrix is a powerful sensitivity based tool that can used to assist in to correction of an initial guess of velocity.[2] The STM can be used to formulate the necessary launch criteria for a ballistic missile in order to make the necessary corrections to hit a target when adjusting to a variety of perturbation methods. The STM can be formulated either through the analytic solutions of motion or accounted for directly by using a numeric sensitivity technique.

We use the STM to determine the sensitivity of the final impact position of the projectile to its initial velocity. We then resolve error by making a velocity correction derived from the state transition matrix. We chose to make our comparison between the method of formulation of the STM by setting up a grid of equally dispersed targets and resolving trajectory solutions from a variety of launch locations.

2 Primary Formulation of the State Transition Matrix

As discussed in Schaub and Junkins, the state transition matrix is a matrix of functions that comprise sensitivities of final states with respect to initial states as in Equation 1. Here we discuss the full blown equation in its raw form.

$$\frac{\partial \boldsymbol{X}(t_{\mathrm{f}})}{\partial \boldsymbol{X}(t_0)} = [\boldsymbol{\Phi}(t_0, t_{\mathrm{f}})] = \begin{bmatrix} \boldsymbol{\Phi}_{11} & \boldsymbol{\Phi}_{12} \\ \boldsymbol{\Phi}_{21} & \boldsymbol{\Phi}_{22} \end{bmatrix} = \begin{bmatrix} \frac{\partial \boldsymbol{r}}{\partial \boldsymbol{r}_0} & \frac{\partial \boldsymbol{r}}{\partial \dot{\boldsymbol{r}}_0} \\ \\ \frac{\partial \dot{\boldsymbol{r}}}{\partial \boldsymbol{r}_0} & \frac{\partial \dot{\boldsymbol{r}}}{\partial \dot{\boldsymbol{r}}_0} \end{bmatrix} \tag{1}$$

$$\boldsymbol{X} = \begin{bmatrix} \boldsymbol{r} \\ \dot{\boldsymbol{r}} \end{bmatrix} \tag{2}$$

$$\delta \boldsymbol{X}(t_{\mathrm{f}}) \approx [\boldsymbol{\Phi}(t_0, t_{\mathrm{f}})] \delta \boldsymbol{X}(t_0) \tag{3}$$

Here $\boldsymbol{X}$ defines the states, in our case position and velocity as shown in 2. We examine the states at two specific times, the initial time, t_0 and final time, t_{f}. This gives us a combination of effects, how small changes in initial position affect final position, $\boldsymbol{\Phi}_{11}$, how small changes in initial velocity affect final position, $\boldsymbol{\Phi}_{12}$, how small changes in initial position affect final velocity, $\boldsymbol{\Phi}_{21}$, and how small changes in initial velocity affect final velocity.

For the ballistic missile problem we only use the sensitivity of the final position with respect to changes in initial velocity, $\boldsymbol{\Phi}_{12}$, thus neglect the other portions of this matrix and refer to $\boldsymbol{\Phi}_{12}$ as the state transition matrix. We resolve the necessary state changes as shown in Equation 3. Later we discuss how this relation can be used in detail to resolve error in where the projectile ends up to where it should be.

This document will show the correlation between the analytical solution and a numerical solution in computing the STM for the advanced ballistic missile problem. A comparison will also be made in the computational effort and trends of convergence or divergence between the two methods for a series of launch points to a fixed array of globally dispersed targets. But first we will examine a detailed examination of the constant gravity ballistic problem.

3 Computation of the STM for a Ballistic Projectile in Constant Gravity

We define our constant gravity vector in a 2-Dimensional plane shown in Figure 1 to be in the y direction. We define constant surface gravity for Earth as -9.81 m/s^2. The vector form of the accelerations for this flat Earth, no drag, no rotation model is shown in Equation 4.

$$\boldsymbol{a} = \begin{bmatrix} 0 \\ g_{0y} \end{bmatrix} \tag{4}$$

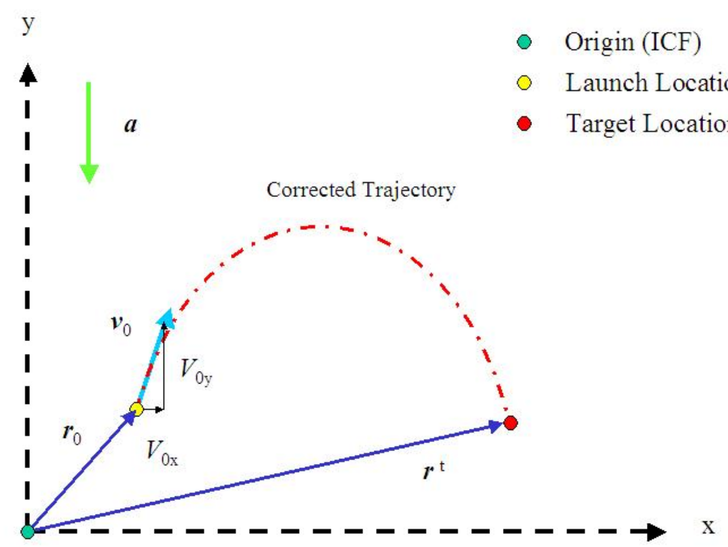

Figure 1: Identification of nomenclature and a representative trajectory to solve the constant gravity problem.

Next, we integrate with respect to time to determine our equations of motion in Equations 5 and 6 for velocity and position respectively.

$$\boldsymbol{v} = \begin{bmatrix} V_{0x} \\ V_{0y} + g_{0y}\Delta t \end{bmatrix} \tag{5}$$

$$\boldsymbol{r} = \begin{bmatrix} r_{0x} + V_{0x}\Delta t \\ r_{0y} + V_{0y}\Delta t + g_{0y}\frac{\Delta t^2}{2} \end{bmatrix} \tag{6}$$

Now we perform the necessary operations to form the state transition matrix, Φ. We utilize the partial derivative to determine the values analytically for the state transition matrix for the constant gravity problem in Equations 7 - 10.

$$\Phi_{11} = \frac{\partial \boldsymbol{r}}{\partial \boldsymbol{r_0}} = \begin{bmatrix} \frac{\partial \boldsymbol{r}}{\partial r_{0x}} & \frac{\partial \boldsymbol{r}}{\partial r_{0y}} \end{bmatrix} = \begin{bmatrix} 1 & 0 \\ 0 & 1 \end{bmatrix} \tag{7}$$

$$\Phi_{12} = \frac{\partial \boldsymbol{r}}{\partial \dot{\boldsymbol{r}}_0} = \begin{bmatrix} \frac{\partial \boldsymbol{r}}{\partial \boldsymbol{r}\dot{_{0x}}} & \frac{\partial \boldsymbol{r}}{\partial \boldsymbol{r}\dot{_{0y}}} \end{bmatrix} = \begin{bmatrix} \Delta t & 0 \\ 0 & \Delta t \end{bmatrix} \tag{8}$$

$$\Phi_{21} = \frac{\partial \dot{\boldsymbol{r}}}{\partial \boldsymbol{r}_0} = \begin{bmatrix} \frac{\partial \boldsymbol{v}}{\partial \boldsymbol{r}_{0x}} & \frac{\partial \boldsymbol{v}}{\partial \boldsymbol{r}_{0y}} \end{bmatrix} = \begin{bmatrix} 0 & 0 \\ 0 & 0 \end{bmatrix} \tag{9}$$

$$\Phi_{22} = \frac{\partial \dot{\boldsymbol{r}}}{\partial \dot{\boldsymbol{r}}_0} = \begin{bmatrix} \frac{\partial \boldsymbol{v}}{\partial \boldsymbol{v}_{0x}} & \frac{\partial \boldsymbol{v}}{\partial \boldsymbol{v}_{0y}} \end{bmatrix} = \begin{bmatrix} 1 & 0 \\ 0 & 1 \end{bmatrix} \tag{10}$$

With Φ we can determine how to resolve a particular target at a particular velocity from a given set of initial conditions. In most cases we would like to just hit our target given an initial guess with a constrained initial position.

For these purposes, we utilize a change in initial velocity to determine the final position and thus concentrate our efforts with Φ_{12}. Here we correct our position with a simple correction.

3.1 Error Resolution

First we use an initial guess to provide us with data on where the projectile lands after a fixed flight time. We can compare the error of where the projectile's impact point on the surface is, $\boldsymbol{r}_f$, to where we should be, $\boldsymbol{r}_f^t$. Equation 11 shows this relationship to determine the range error $\delta \boldsymbol{r}_f$.

$$\delta \boldsymbol{r}_f = \boldsymbol{r}_f - \boldsymbol{r}_f^t \tag{11}$$

After we have the error vector, we can now find the velocity correction using Φ_{12}.

3.2 Velocity Correction

With Φ_{12} and $\delta \boldsymbol{r}_f$ we can backsolve to find the necessary velocity correction vector, $\delta \boldsymbol{v}$ as shown in Equation 12.

$$\delta \boldsymbol{v} = [\Phi_{12}]^{-1}[-\delta \boldsymbol{r}_f] \tag{12}$$

The velocity corrected vector $\delta \boldsymbol{v}$ is then added to the initial velocity vector set to make the correction and precisely hit the target.

3.3 Example Velocity Only Correction Constant Gravity Projectile

We define our initial conditions $X(t_0)$ as follows: $r_{0x} = 0$ m, $r_{0y} = 0$ m, $V_{0x} = 5$ m/s, $V_{0y} = 3$ m/s. And define our final conditions $X(t_f)$ as follows: $r_x^t = 5$ m, and $r_y^t = 20$ m. Lastly we define our time of flight Δt as 5 seconds.

We use these initial conditions with our equations of motion to determine where our projectile lands after the time of flight, $\boldsymbol{r}_f$. Then we use Equation 11 to resolve the error vector $\delta\boldsymbol{r}_f$. We find it to be as follows:

$$\delta\boldsymbol{r}_f = \begin{bmatrix} 20.0000 \\ -127.6250 \end{bmatrix} m \tag{13}$$

Next we use Equation 12 to apply the necessary velocity correction, $\delta\boldsymbol{v}$ to resolve the target. The result is plotted in Figure 2.

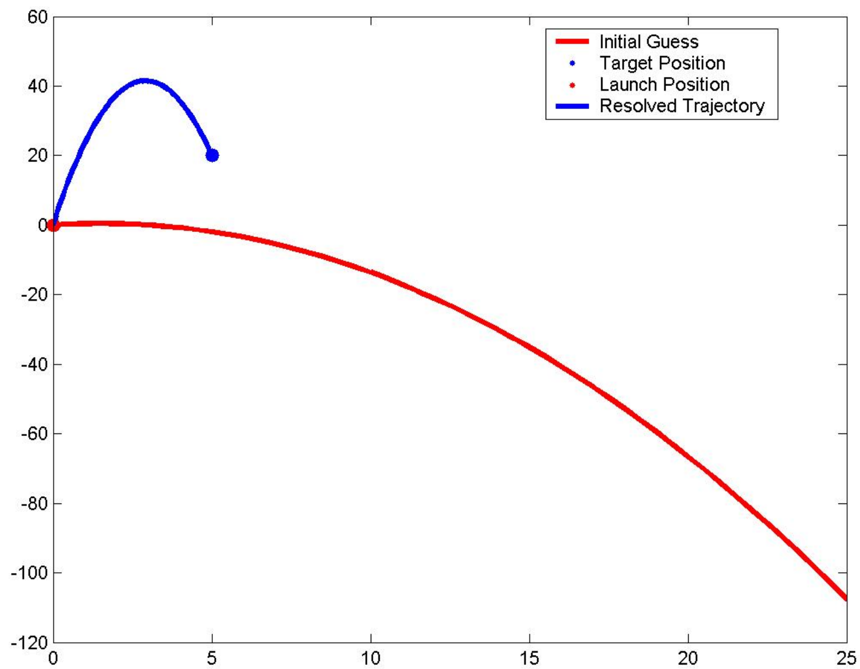

Figure 2: Corrected Trajectory uses Φ_{12} to change initial velocity to strike target.

Examining the error vector following the correction and using the equations of motion to resolve the final position, we find that it is exactly zero. With no perturbations to the system and being in a constant acceleration environment this result makes sense.

4 Methods to Compute Φ_{12} for the Ballistic Missile Problem

The state transition matrix provides a method for mapping the initial state vector of a system to a final state vector at any particular time. Corrections must be made to the initial velocities in order to minimize induced effects on trajectories. This document resolves effects due to drag on the projectile as well as accounting for a spherical rotating Earth.

There are two primary methods for computing such initial velocity corrections: the analytic solutions for determining where a body will be given an initial guess as well as the final portion of the initial guess; and the numerical solution where by a sensitivity of the trajectory to small velocity variations from the initial guess are computed.

4.1 Analytic Method

The analytic method[3] employs the special case compilation of terms from the F and G solution of propagating a two-body problem, or Keplerian motion, found in Equation 14. Here we no do not account for any perturbations or non-linearities in the system. The only effects considered in this analytic method are the inverse square law gravity effects. As in the example STM calculation, we require initial position, initial velocity, and time of flight. We also require the resultant position and velocity that results from the initial state.

$$
\begin{aligned}
[\Phi_{12}] =& \frac{r_0}{\mu} \cdot (1-F)\left(\begin{bmatrix} \Delta r_x \\ \Delta r_y \\ \Delta r_z \end{bmatrix} \begin{bmatrix} V_{0x} & V_{0y} & V_{0z} \end{bmatrix} - \begin{bmatrix} \Delta V_x \\ \Delta V_y \\ \Delta V_z \end{bmatrix} \begin{bmatrix} r_{0x} & r_{0y} & r_{0z} \end{bmatrix} \right) \\
&+ \frac{C}{\mu} \left(\begin{bmatrix} V_x \\ V_y \\ V_z \end{bmatrix} \begin{bmatrix} V_{0x} & V_{0y} & V_{0z} \end{bmatrix} \right) + G \begin{bmatrix} 1 & 0 & 0 \\ 0 & 1 & 0 \\ 0 & 0 & 1 \end{bmatrix}
\end{aligned} \tag{14}
$$

Where F and G are the terms from the F and G solution represented in Equations 15, 16, and 17; and C is represented in Equation 18.

$$F = 1 - \frac{r}{p}(1 - \cos(\Delta f)) \tag{15}$$

$$G = \frac{r_0 r \dot{F}}{\sqrt{\mu a}} \tag{16}$$

$$\dot{F} = \sqrt{\mu p} \tan\left(\frac{\Delta f}{2}\right)\left(\frac{1-\cos(\Delta f)}{p} - \frac{1}{r_0} - \frac{1}{r}\right) \tag{17}$$

$$C = a\sqrt{\frac{a^3}{\mu}}(3\sin(\hat{E}) - (2 + \cos(\hat{E}))\hat{E}) - \Delta ta(1 - \cos(\hat{E})) \tag{18}$$

$$\hat{E} = \arctan\left(\frac{\frac{-r_0 r\dot{F}}{\sqrt{\mu a}}}{1 - \frac{(1-F)r_0}{a}}\right) \tag{19}$$

Where $\hat{E}$ is the modified eccentric anomaly in Equation 19, a is the semi-major axis, p is the semilatus rectum, f is the true anomaly angle, and Δt is the flight time of the projectile. For our simulation, we derive a and p from a mapping of the cartesian coordinate set to its orbital elements and use the definition of the dot product to compute the change in true anomaly angle, Δf, between the location of the target and the launch location. We utilize the two-body solution's launch position, $\boldsymbol{r}_0$, and velocity $\boldsymbol{V}_0$ as well as the arrival position, $\boldsymbol{r}$, and velocity, $\boldsymbol{V}$, to compute the changes in position and velocity. These calculations use the form of subtracting the launch conditions from the target conditions.

4.2 Numerical STM

The numerical STM is determined by adding small changes in velocity to the initial cartesian state.[2] These changes are represented as vector quantities. For instance Equation 20 demonstrates a small change, v_ϵ in velocity in the cartesian inertial x direction where v_ϵ is 0.001 km/s.

$$\delta\boldsymbol{v}_1 = \begin{bmatrix} v_\epsilon & 0 & 0 \end{bmatrix} \tag{20}$$

A change in each of the cartesian directions is added to the reference cartesian state. Each is then forward propagated for a predetermined flight time whereby a final location is resolved for the three cases of velocity variation. These final locations are then compared to the reference cartesian state's resultant final position, $\boldsymbol{r}_{\text{ref}}$, as depicted in Figure 3.

Sensitivities are then derived by dividing the change in range over the magnitude of the variation in velocity. Equation 21 indicates the calculation for the first column of the STM. Here, Target i, for $i = 1, 2, 3$, from Figure 3 is indicated as $\boldsymbol{r}_f^i$ and the reference final location is $\boldsymbol{r}_{\text{ref}}$.

$$\begin{pmatrix} \frac{\delta r_x}{\delta v_i} \\ \frac{\delta r_y}{\delta v_i} \\ \frac{\delta r_z}{\delta v_i} \end{pmatrix} = \frac{\boldsymbol{r}_f^i - \boldsymbol{r}_{\text{ref}}}{v_\epsilon}. \tag{21}$$

The numerical sensitivity matrix is then formed as shown in Equation 22 by utilizing the three varied final projectile locations formed by propagating the perturbed initial conditions along the flight time.

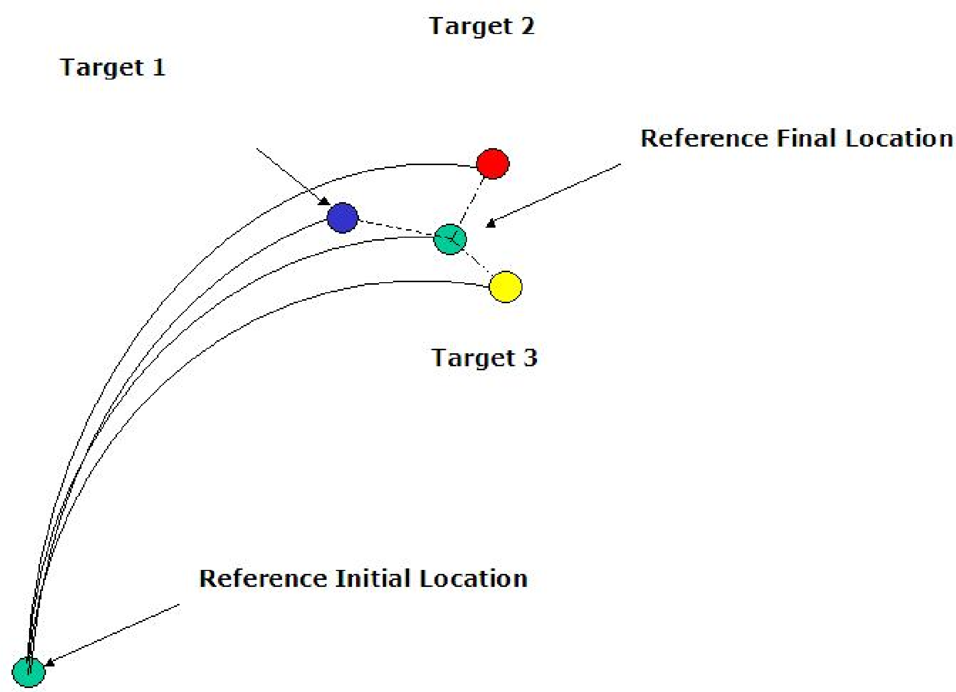

Figure 3: Numerical STM compares a reference trajectory final location to 3 perturbed trajectories.

$$[\Phi_{12}] = \begin{bmatrix} \frac{\delta r_x}{\delta v_1} & \frac{\delta r_x}{\delta v_2} & \frac{\delta r_x}{\delta v_3} \\ \frac{\delta r_y}{\delta v_1} & \frac{\delta r_y}{\delta v_2} & \frac{\delta r_y}{\delta v_3} \\ \frac{\delta r_z}{\delta v_1} & \frac{\delta r_z}{\delta v_2} & \frac{\delta r_x}{\delta v_3} \end{bmatrix} \tag{22}$$

Problems using the numerical STM involve the creation of a singular matrix. These singularities are introduced when the sensitivity in range is computationally negligible with respect to the small change in velocity. These instances can occur when the projectile is sent on a hyperbolic trajectory. A critical velocity loop exception is introduced to the program to account for these effects.

Further, we must use constant flight time when using the numerical STM. Propagators can be set up in order to utilize the constraint of the surface in order to determine a time of impact. With perturbations in velocity, the flight time for each case will differ. This would imply that the STM is also a function of time, which it is not. Instead, a constant flight time propagation technique must be invoked regardless of whether the projectile's final perturbed position is above or below the surface. However, to determine the reference position of the projectile, $\boldsymbol{r}_{\text{ref}}$, the trajectory is propagated until a surface hit is observed. This assures that the projectile will hit the surface if not on an escape trajectory and thus all solutions are found in a ring on the surface and not just within a sphere.

The forward propagation technique in a purely numerical STM is a numerical method using numerical integration that accounts for the atmosphere and the projectile's ballistic coefficient. This numerical solution uses a propagation technique that accounts for all effects encountered by the projectile while on its path as defined by the forward propagation technique. Therefore it appears to be more robust than pure analytical methods when for accounting for drag and other perturbations.

5 Use of the ODE45 Numerical Integrator with Event Detection

The ODE45 numerical integrator is one of many built-in functions in the Matlab software library. ODE45 is considered to be an accurate means of integration because it uses an internally variable time step in order to resolve the solution to a desired accuracy as defined by the user. The user must also recognize that because the steps are variable, this will induce a conditional environment that may alter results of a complex environmental model.

The defined atmosphere used in this simulation is such that the atmosphere is invoked when on the rising portion of the trajectory above a 122 km altitude and remains on until impact. In order to satisfy this condition, the previous height on the downward portion of the trajectory below 122 km must be greater than the current height.

Caution must be observed when using the propagator as the previous steps are compared due to the nature of ODE45 actually proceeding backwards in time and stepping with smaller increments forward in time. When computational time becomes extreme and solutions are not determined after multiple minutes, its entirely possible that the the atmosphere is being turned on and off, making it extraordinarily difficult for ODE45.

Two methods of ODE45 can be used, a fixed time approach going from some initial state to some final state with an undetermined number of points in between. This is useful for setting a very large time and having the event detection option find the impact point and flight time. Therefore a constant for final time is used throughout and actual flight time is extracted using the event detection method. For use in computing the sensitivity matrix of the numerical model, a constant flight time is used to compare how the changes in the initial state affect the final state. Thus, events detection is no longer utilized in this operation.

Alternative forms of numerical integration can be utilized in the future, but detailed analysis would need to occur to determine the impact point location and tolerances explored.

6 Problem Definition

It is desired to formulate the necessary initial conditions of velocity for a given initial surface location and a desired final target location in the Earth fixed frame of reference. The initial position and velocity vectors are then propagated throughout the flight time of a simulated point-mass projectile until impact. An initial guess is computed using the Keplerian two-body solution for flight time and initial velocity. Various methods including the F and G solution and Keplerian orbit plane determination are available for computing this solution and will not be reviewed here. This guess is then subjected to the state transition matrix technique and velocity corrections are applied. In order to determine a measure of effectiveness for each type of state transition matrix a host of globally dispersed targets is composed and convergence criteria such as number of iterations to converge (if at all) and computational time is compared for a variety of launch locations.

6.1 Non-Keplerian Effects

Numerous non-Keplerian motion effects can be added to increase the fidelity of the ballistic missile problem model. Some of the major effects due to the environment will be resolved in this study including planetary rotation and the atmosphere on a simple projectile with a defined ballistic coefficient. This projectile will not have a defined an inertia tensor nor will lift be modelled.

6.1.1 Rotation

Planetary rotation is a significant source of error for projectiles with long flight times. As the body rotates, the target itself will move. For minimum energy two-body trajectories, the flight time can remain constant, and a new trajectory computed to essentially lead the target.[4] However, since the purpose of these simulations is to build tools capable of resolving higher fidelity solutions, the minimum energy transfer time is not used to form solutions; it is used as an initial guess only.

For the purposes of this study, we employ the local sidereal time, γ_t. Knowing the reference Greenwich sidereal time, γ_{UT}, we can rotate the Earth to the target's longitudinal position, λ^t, of the Earth frame to the inertial frame. Then we account for the rotation of the Earth during the flight time of the projectile shown in Equation 23.

$$\gamma_0^t = \gamma_{\mathrm{UT}} + \lambda^t \tag{23}$$

We then propagate the local sidereal time as shown in Equation 24.

$$\gamma_f^t = \gamma_0^t + \omega_{\mathrm{Earth}} \Delta t \tag{24}$$

The remaining step is to now determine the target location in inertial coordinates.

$$\boldsymbol{r}^t = R_{\text{Earth}} \begin{bmatrix} \cos(\phi^t)\cos(\gamma_f^t) \\ \cos(\phi^t)\sin(\gamma_f^t) \\ \sin(\phi^t) \end{bmatrix} \tag{25}$$

Here we find the final inertial position of the target $\boldsymbol{r}^t$ used in Equation 30 using for the first time, the latitude location of the target, ϕ^t.

We also note that the launch site has an initial inertial velocity that will translate to a different "real" launch velocity due to the Earth's rotation. We expect that it is less expensive to launch east than to launch west in these cases since we already have an initial eastward velocity. Further discussion of this topic will be reviewed in the trajectory analysis section.

6.1.2 Atmosphere

A piece-wise exponential model was selected from previous work,[5] to represent the atmosphere. It is assumed that an exponential density model can accurately represent the atmosphere.[1,6,7] The nature of exponential atmosphere density model provides the ability to estimate the density at altitude and obtain closed-form solutions while maintaining reasonable accuracy. However, since the analysis will be performed numerically, any model can be utilized. We choose to use this model due to its availability and understanding of its inherent error with respect to the 1976 Standard Atmosphere. For sea-level conditions we assume a initial density, ρ_0 of 1.225×10^9 kg/km^3.

For this exponential model the term Γ will be used to represent the density ratio at altitude as shown in Equation 26.

$$\Gamma = \frac{\rho}{\rho_0} = e^{\frac{-h}{\Lambda}} \tag{26}$$

The piecewise function changes properties at 152 km altitude (500,000 ft.) For the upper segment of the piecewise function, the reference density ratio at 1.524×10^2 km is 1.4848 kg/km^3. A scale height, Λ for elevations from 0 to 152 km is 6.882 km. For 152 km and above, 83.887 km is used. In Figure 6.1.2 we see the comparison of the 1976 Standard Atmosphere Model with that of the comprised piecewise exponential density function. For low altitudes we see there is good agreement with a general trend following the higher altitude portion that otherwise would be neglecting a far greater portion of density if a single relation was used.

This study invokes the atmosphere at 122 km (400,000 ft.) on the rising portion of the trajectory through the descent phase to the surface. It is assumed the the trajectory on the ascending portion to this altitude location of 122 km follows a Keplerian trajectory using thrust to match the necessary conditions when drag begins to be

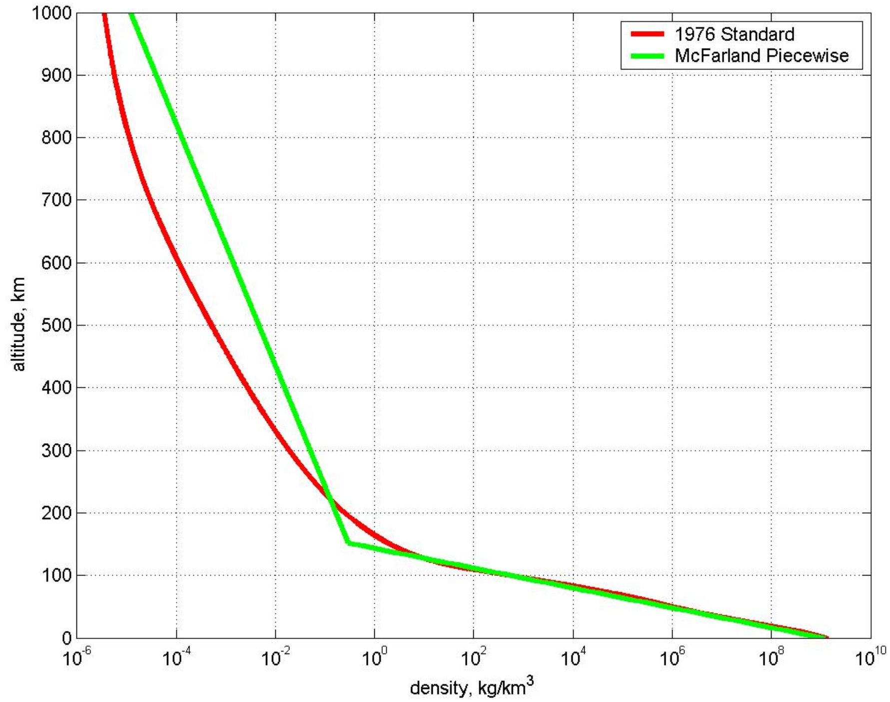

Figure 4: A plot of density vs. altitude comparing the 1976 Standard Atmosphere to the McFarland model[5] employed in this simulation.

modelled. Thereafter drag is employed throughout the trajectory until impact on the surface.

6.1.3 Projectile Definition

The next task is to model a vehicle. This vehicle has three key parameters that we must know in order to determine the influence of drag acceleration. They are mass, representative area, and drag coefficient. In many cases all three of these parameters are not constant. A vehicle with an ablative heat shield will lose mass; a vehicle could deploy speed brakes or a parachute to increase area; drag coefficient is generally a function of lift coefficient which varies with Mach number and angle of attack to include some of the variations. For our discussion, we model a ballistic missile; thus we neglect lift terms and consider drag to be much greater than lift and consider drag coefficient and area to be constant.[1]

When mass: m, area: S, and drag coefficient: C_D are combined they represent a term called the ballistic coefficient,[8] β. This is represented as $\frac{m}{C_D \cdot S}$, and is traditionally in units of kg/m^2.

To maintain unit consistency throughout the simulation, we will redefine the units as kg/km^2. The ballistic parameter, β for satellites is considered low[8] at values of 20×10^6 kg/km^2 and high for 200×10^6 kg/km^2. Feathers for instance have a very low ballistic parameter, while a battleship projectiles and ballistic missiles have large values. This is the parameter that defines how well a projectile can penetrate the atmosphere.[9] For the purposes of this study, four values of β are chosen in $\frac{\text{kg}}{\text{km}^2}$: ∞, to indicate that the projectile is unaffected by the atmosphere; 2×10^{12}; 2×10^9, and 200×10^6. Realizing that these values are not wholly representative of probable objects and that values of β are not constant, but fundamental to the introductory examination of the effects of drag. Ballistic missiles by design will attempt to penetrate the atmosphere, so lower values are not realistic. Next we determine the method in which we model drag.

6.1.4 Modeling Drag

The drag force is generally defined[1] as in Equation 27.

$$D = \frac{1}{2}\rho v^2 C_D S \tag{27}$$

Where D is drag force and v is velocity magnitude. To incorporate the more advanced vector form of acceleration, we divide by mass and multiply by the negative velocity direction unit vector as shown in Equation 28.

$$\boldsymbol{a}_{\text{Drag}} = \frac{1}{2}\rho(\boldsymbol{v}\cdot\boldsymbol{v})\frac{C_D S}{m}\frac{(-\boldsymbol{v})}{\parallel \boldsymbol{v} \parallel} \tag{28}$$

Next we simplify the equation and incorporate β in 29.

$$\boldsymbol{a}_{\text{Drag}} = \frac{\rho}{2\beta}(\boldsymbol{v}\cdot\boldsymbol{v})\frac{(-\boldsymbol{v})}{\parallel \boldsymbol{v} \parallel} \tag{29}$$

Now that rotation, drag, and the projectile are defined, we have the tools setup to produce a trajectory solution. Now we examine how to compare error and make corrections to the initial state.

6.2 Error Resolution

We can compare the error of where the projectile's impact point on the surface is, $\boldsymbol{r}_f$, to where we should be, $\boldsymbol{r}_f^t$. Previously in the rotation section we discussed how to determine where the target will be on the surface of the Earth after the given flight time. We can compare our forward propagated solution's impact location in Equation 30 to the target location to determine the range error $\delta\boldsymbol{r}_f$.

$$\delta\boldsymbol{r}_f = \boldsymbol{r}_f - \boldsymbol{r}_f^t \tag{30}$$

For target locations on the poles for pure rotation solutions, we expect the answer to be the same as the two-body solution for the spherical body. With the addition of drag and other perturbations to the problem, the non-linear dynamics of the system will alter this and must be corrected.

6.3 Velocity Correction

With $[\Phi_{12}]$ and $\delta \boldsymbol{r}_f$ we can backsolve to find the necessary velocity correction vector, $\delta \boldsymbol{v}$ as shown in Equation 31.

$$\delta \boldsymbol{v} = [\Phi_{12}]^{-1}[-\delta \boldsymbol{r}_f] \tag{31}$$

The velocity corrected vector $\delta \boldsymbol{v}$ is then added to the initial cartesian velocity vector set to correct for the effects of the perturbation. After successive iterations of re-computing the final location of the trajectory after applying the correction, the error vector $\delta \boldsymbol{r}_f$ is driven to zero when the solution converges; else it diverges.

7 Problem Solving Method

We design a scheme to approach the formulation of the ballistic missile trajectory. First we identify that the two-body Keplerian solution is valid for a non-rotating Earth with no atmosphere. Next in this method we specify that the minimum energy semi-major axis will be employed. We hypothesize that we can correct this initial guess for a trajectory by employing the state transition matrix method for the ballistic missile problem by correcting the initial velocity to resolve the appropriate final impact location of the projectile within a tolerance.

As shown in Figure 5 the program receives inputs of launch site and target site initial conditions.

The program receives inputs of launch site and target site initial conditions. The two-body no-rotation solution is then processed. A flight time and initial cartesian coordinate set are outputted to a propagator to create the full trajectory profile. The target location on the Earth's surface is then rotated the appropriate amount that occurs during the time of flight, and error is compared. If error is less than the predetermined tolerance, the function halts and a trajectory is resolved. Otherwise, the program continues to resolve a solution.

When a solution is not within the predetermined tolerance, the initial guess trajectory state is outputted to the STM of choice. The error vector of the rotated target to the final projectile's location after the time of flight is compared in the while loop. Then the velocity correction is made. The new trajectory initial conditions are then forward propagated until the projectile impacts the surface of the Earth. We then rotate the target location and again compare error.

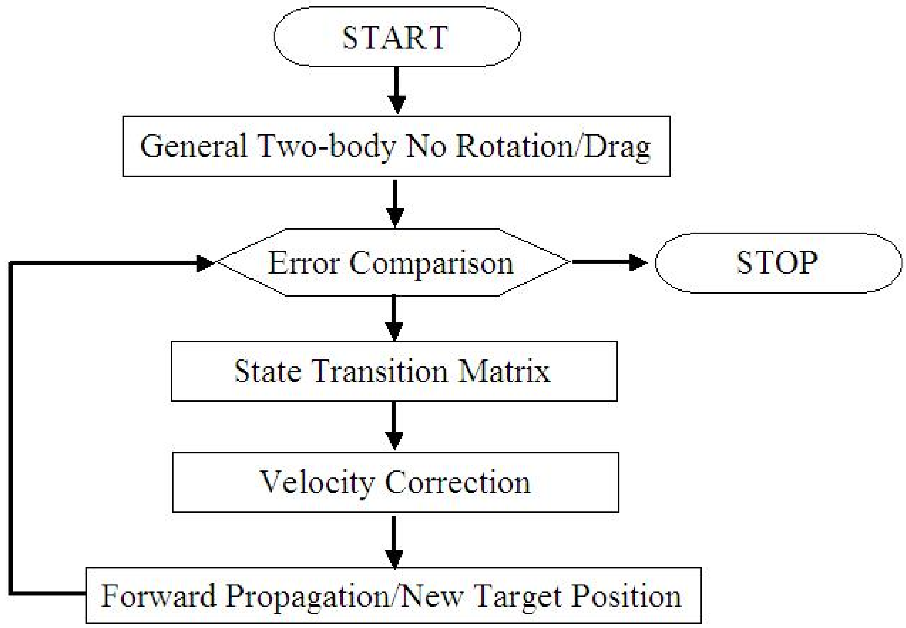

Figure 5: Iterative approach used to resolve solution.

We setup a counter to determine the number of iterations required to correct the velocity of the cartesian state to resolve a solution within tolerance. A predetermined ejection criteria is also put in place to account for diverging solutions or situations such as the 180° case where the minimum energy semi-major axis is actually the radius of the Earth. For this situation, large difficulties arise when correcting velocity due to the surface impact constraint and another initial guess will be researched for this region of cases.

7.1 Representative Solution

A representative case that uses a single surface launch and target location is used to demonstrate the model and its capabilities. Here we use $\phi_0 = 0^{\circ}$ N and $\lambda_0 = 80^{\circ}$ E. The target location for this exercise is $\phi^t = 50^{\circ}$ S and $\lambda^t = 150^{\circ}$ W. We arbitrarily chose a STM since we are not sure yet of how each will perform. In the case of the two-body trajectory; no velocity correction at all is performed; the loop is directly exited. We also examine pure rotation and rotation and drag cases. Each of these solutions examine the trajectories followed.

Figures 6(a) and 6(b) show a comparison of the ground tracks traced over the surface of the rotating Earth during the time of flight of a projectile with $\beta = 200\times10^6$ kg/km^2. In Figure 6(a) we see the entire profile. We note that the two body solution is displaced westward, as we should expect for Earth rotation. We also note that the drag and rotation solution are similar to the rotation only solution. This also means that rotation effects are much greater than those caused by drag. This result was not entirely expected but makes sense when examining the similarity between the trajectories. We find that the drag and rotation trajectory leads the target slightly, prior to atmospheric entry, to account for the velocity slow down that results from the atmosphere.

Figure 6(b) we see a view of the Earth constrained to the target site. Here we notice that there is a significant deviation from the flight path of the drag and rotation solution from the rotation solution. We note that each marker indicates the position of the projectile with 1 second increments. The drag case is shown to have a significant compression of these steps and a westward motion into the target. We thus expect that the inertial speed of the projectile as it falls through the denser portion of the atmosphere is actually now moving at a slow enough rate that the Earth's relative rotation speed is significant. Here we also note that the distances between the markers for the rotation and two-body solutions are similar. This indicates that these solutions during this period of time are approximately travelling at the same velocity.

We can therefore expect that the rotation correction solution and the drag solution should be fairly similar in the amount of necessary initial velocity correction. This is due to the resultant inclination chosen to reach the target, and the observation that the trajectories do not vary in an extreme manner throughout, we do notice that the flight time for the drag case is longer for this case, therefore even more Earth rotation will occur in this situation than just the pure rotation case.

We demonstrate this fact by examining the time vs. altitude plot shown in Figure 7(a). We see that there is approximately 10% difference between the time of flight of the drag and rotation case to the cases without an atmosphere. This increase is a direct result of slowing down in the significant atmosphere. We can determine that the time of entry is about 300 seconds long for this case which also makes sense.[1]

We also note that the apogee altitude varies significantly between these cases. A point of interest is that as rotation effects increase the trajectory's apogee altitude decreases. This appears to be a correlation that the angular distance between the launch location and the final location of target after the time of flight is a small distance when launching westward. This thus results in a lower apogee altitude.

We also wish to examine conditions upon re-entry into the Earth's significant atmosphere at 122 km. We examine the plots from the downward portion of the trajectory only, as indicated by the arrows in Figures 7(b) and 7(c). In Figure 7(b) we discover a significant deviation in the scalar inertial velocity of the projectile as it falls through the atmosphere. This correlates directly to the compressed time step formation indicated in Figure 6(b) as well as the increased flight time as indicated in Figure 7(a). We also note that the peak acceleration for this trajectory and value of β is about 40 G's. Where the units "G" are the surface acceleration of the Earth's gravity generally approximated as 9.81 m/s^2. We expect that for larger values of β the velocity profile trend more to the two-body and pure rotation cases with maximum acceleration decreasing.

8 Comparison of STMs for Use in Resolving Trajectories for an Array of Targets

Now that we have a feel for how solutions are formed for a single trajectory case, we form a array of target locations and an array of launch locations. These array are used to demonstrate the effectiveness of each type of method for resolving the trajectory for any desired launch or target location. We compare the numerical formulation with the analytical formulation of the STM for each of these cases to determine which is better for this specific application of the ballistic missile problem. We can also determine whether it is better to compute the STM just once outside the iteration loop or if it is more effective to utilize the STM inside. From the detailed examination of the representative solution, we expect that the analytical method should be sufficient to account for the Earth rotation and drag effects. The entry portion of time of flight is small when compared to the time of flight for the full trajectory, and it appears to be compensated for with more rotation of the Earth.

8.1 Array of Targets

An array of targets was formulated using a grid work of points in latitude and longitude. Initial studies including rotation utilize a 703 point array ranging from 90° N latitude to 90° S latitude in increments of 10°. A longitudinal grid from -180° to 180° E is formulated also using increments of 10°. This results in 658 unique data points for examination when accounting for the overlap that occurs numerically at the poles and 180°.

For cases employing drag, a much smaller grid size of 49 points is used due to the much heavier computational requirements. This grid is defined from 90° N to 90° S in increments of 30° with longitude from 90° W to 90° E by increments of 30°. Shown in Figures 8(a) and 8(b) is the target array with 37 unique points with respect to the surface of Earth.

The drag case grid size reduced in longitudinal span to eliminate the large errors associated with the two-body solution initial guess and account for increased computational time required to formulate the solutions.

8.2 Array of Launch Locations

Launch locations were chosen with strict regard to the assumption of symmetry across the equator. The initial locations of the representative launch locations are chosen to be 0° N by 0° E, 45° N by 0° E, and 90° N by 0° E. Figures 8(a) and 8(b) indicate the launch locations.

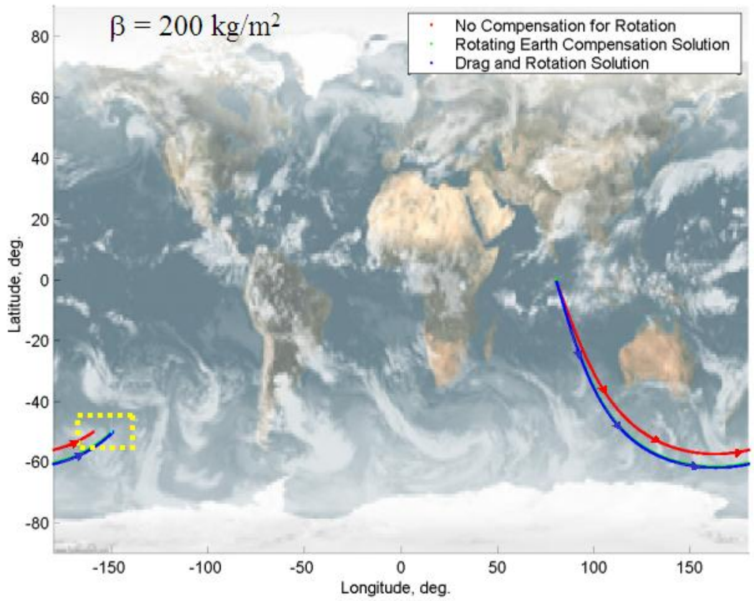

(a) Global groundtrack of solutions.

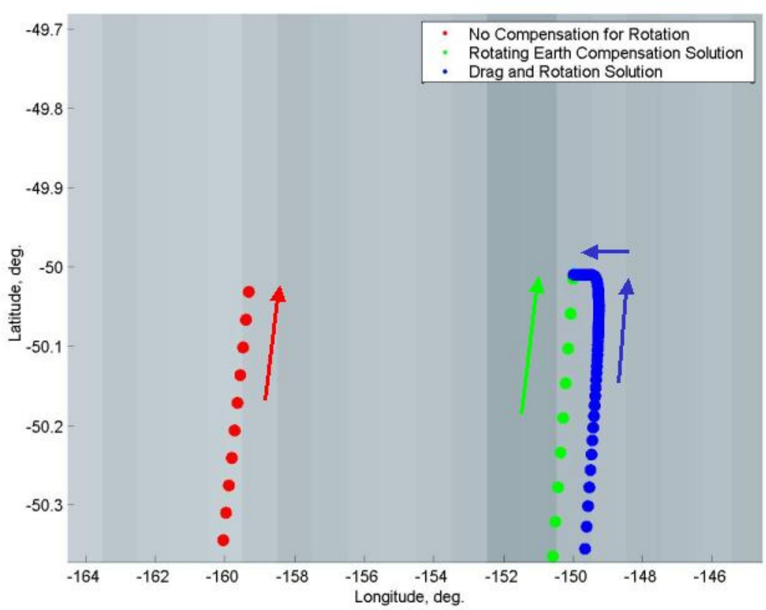

(b) End of trajectory detailed examination of groundtrack.

Figure 6: Groundtrack of solutions for two-body motion(no atmosphere or rotation used in calculation), pure rotation(no atmosphere used in calculation for in trajectory), and drag and rotation cases($\beta = 200 \times 10^6$ kg/m^2)

.

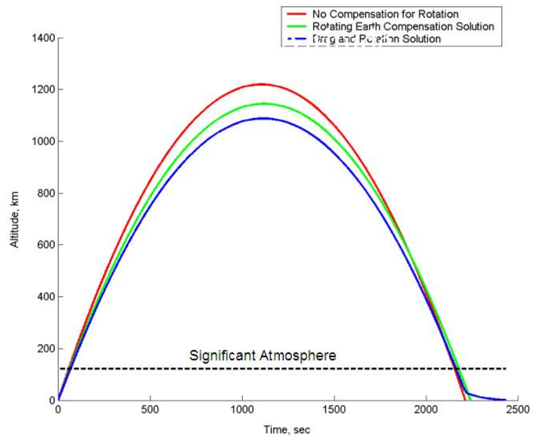

(a) Time vs. Altitude

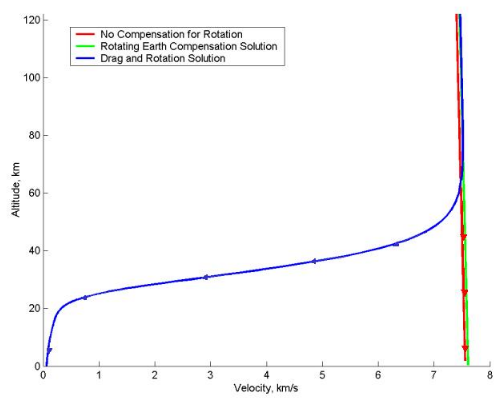

(b) Velocity vs. Altitude

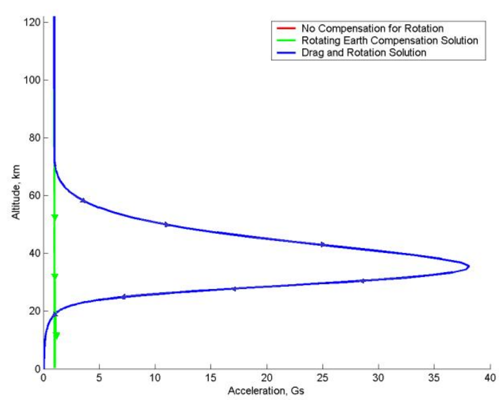

(c) Acceleration vs. Altitude

Figure 7: Plots of projectile dynamics for various levels of modelling fidelity.

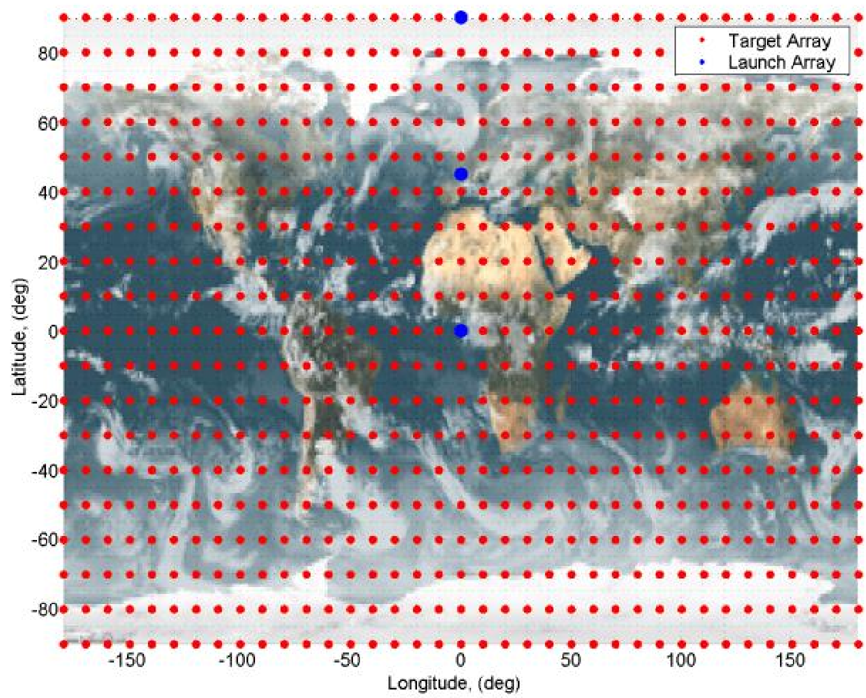

(a) Rotation Array

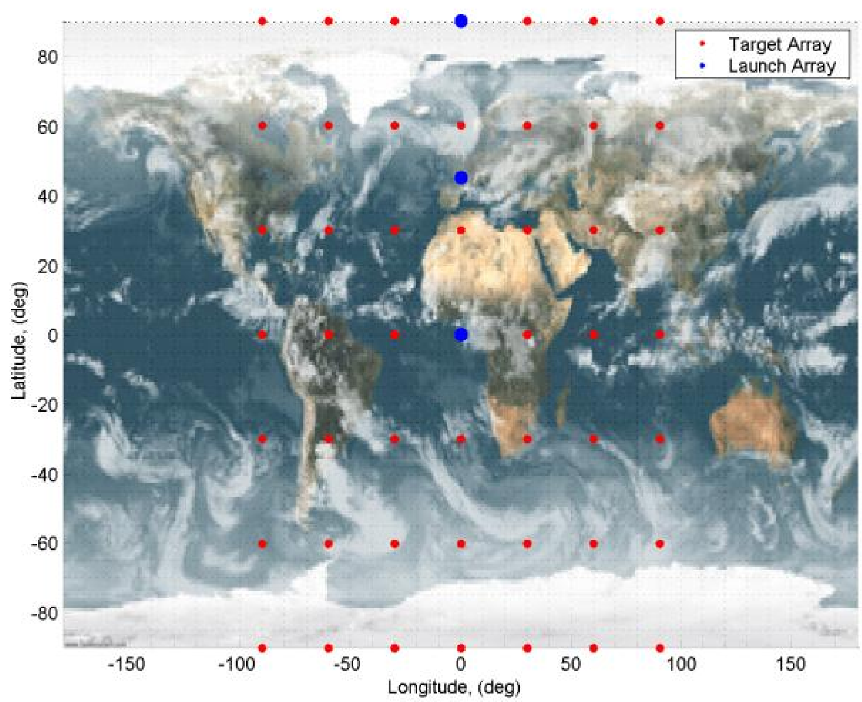

(b) Rotation/Drag Array

Figure 8: Array of Targets and Launch Locations for differing levels of fidelity.

8.3 Measures of STM Effectiveness

The primary means of comparing the numerical and analytical STM effectiveness is chosen to be the number of iterations required to correct the velocity. The number of iterations results in the indirect comparison of the computational power required in order to resolve a solution. An outline of the program created to solve the problem is shown in Figure 5.

It was chosen that 10 iterations would be allowed for velocity corrections to resolve the target solution within an accuracy of 1.6 km (recall this error is a linear error that is the direct subtraction of vectors from the target location to the final location of the projectile). Solutions that did not converge with this number of iterations are given a value of 10. If solutions began to diverge or exceeded the critical velocity, a value of of the last iteration plus 10 is assigned.

The solutions are further examined using the time required to attempt a solution for each grid point. This examination is subjective, however, to the available computing resources and is not directly repeatable. Solutions are examined as far as determining the inclination of the suborbital trajectory's plane and the angular distance between surface locations in order to determine discontinuities. These discontinuities would result when solutions would fail to converge and errors are large. When drag is introduced, the computational requirement is observed to increase by nearly three orders of magnitude, and rate of divergence rapidly increases.

8.3.1 Critical Velocity Loop Ejection Criteria

A critical velocity requirement is necessary to prevent numerical simulation of a hyperbolic trajectory. These trajectories will never fall back to the surface of rotating body, and thus will always fail to converge. Here critical velocity[2] is defined as Equation 32 where R_{Earth} is the radius of the spherical body.

$$V_{crit} = \sqrt{\frac{2\mu_{\text{Earth}}}{R_{\text{Earth}}}} \tag{32}$$

Using this requirement, resultant corrected velocities exceeding the critical velocity will result in the iteration loop termination and a value of 10 added.

8.4 Use of the STM for Resolving the Trajectory

Previously we introduced the numerical and analytic forms of the STM. We expect the analytic form to be computationally faster due to the fact that effects of drag are not included in its formulation. We are not certain as to whether which solution converges faster in the number of iterations required however, or if there are regions where solutions cannot be resolved. We examine 4 separate methods in this analysis: the external analytic(EA) STM, the internal analytic(IA) STM, the external numeric(EN)

STM, and the internal numeric(IN) STM to determine convergence properties to resolve the ballistic missile trajectory.

8.4.1 Internal Methods

An approach was conceived to determine whether a reformulation of the STM would be appropriate and even assist increasing the speed in which the process would resolve a solution. Here the STM is calculated inside the iteration loop shown in Figure 5. The process reevaluates the sensitivities at each iteration correcting the velocity at each step using this new sensitivity.

8.4.2 External Methods

Techniques placing the analytical and numerical solutions merely outside the iterative loops are also examined. These external methods employ the STM prior to the internal processing loop of the velocity correction and internal comparison of error. In other words, we compute one STM instead of determining the sensitivities in succession which reduces required computational power per iteration at the sacrifice of accuracy.

8.5 Rotation Effects

The addition of rotation is the first level of complexity added to the basic ballistic missile problem. Target sites will move as the Earth rotates during the period of flight. These target sites therefore must be led in the inertial frame in order to hit them after the missile's time of flight. Thus, pure rotation is seen as a good baseline for an initial comparison, and this method is employed to determine what the final coordinates of the target location are after the flight time of the vehicle. This method is used throughout the simulation as flight time is refined to reflect the flight time necessary to hit inside the target ring of accuracy. With our tools we have constructed, we initiate our simulation with $\beta = \infty$ to account only for the rotational effects of Earth during the projectile's flight.

8.5.1 Uncorrected Two-Body Solution for $\beta = \infty$

First we examine what amount of error we expect from our initial guess using the two-body solution with no velocity correction. This will determine how accurate our guess is an can gain insight into the reasons for potential failure of the STM to resolve a trajectory within the predetermined tolerance of impact error.

Shown in Figure 9(a) we see that the scalar range error, δr exceeds over 1000 km when nearing 180° of angular distance shown in Figure 11(a).

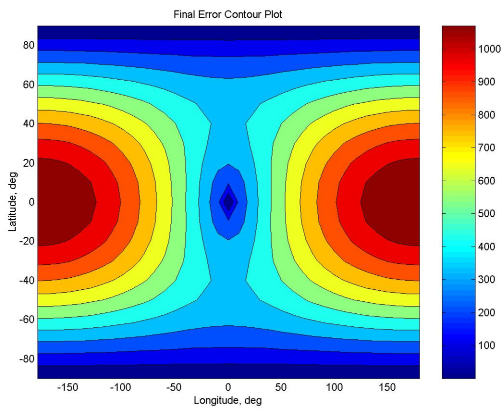

(a) $\beta = \infty$

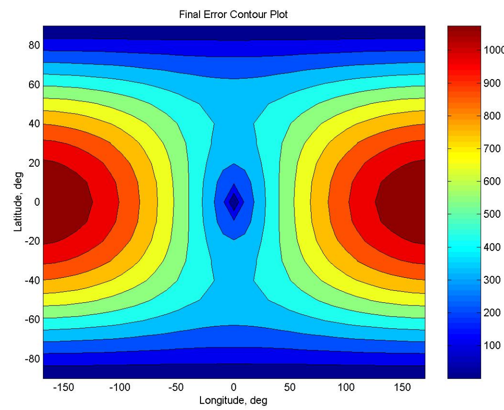

(b) $\beta = 2 \times 10^{12}$

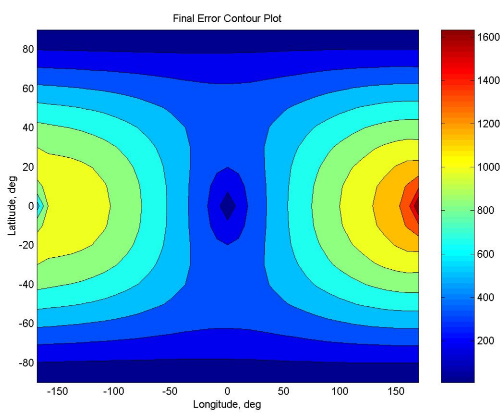

(c) $\beta = 2 \times 10^9$

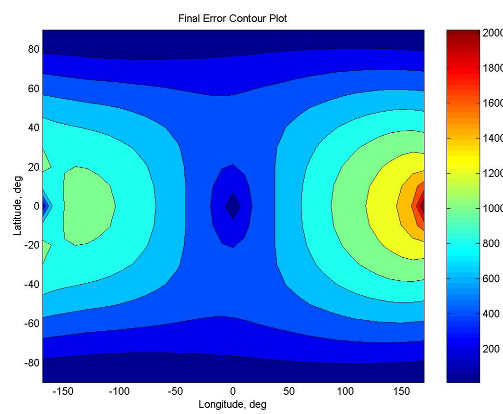

(d) $\beta = 200 \times 10^6$

Figure 9: Error contour plot for launch location 0° N 0° E for solutions uncorrected initial velocity provided by the two-body solution. This plot contains data for the 703 point target array.

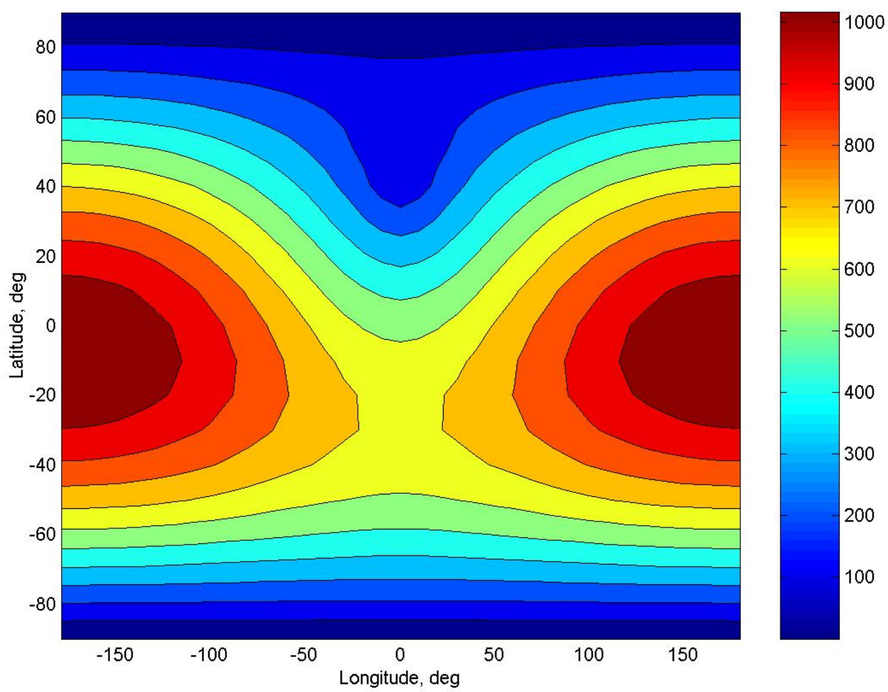

Figure 10: Error contour plot for launch location 45° N 0° E for solutions uncorrected initial velocity provided by the two-body solution. This plot contains data for the 703 point target array $\beta = \infty$.

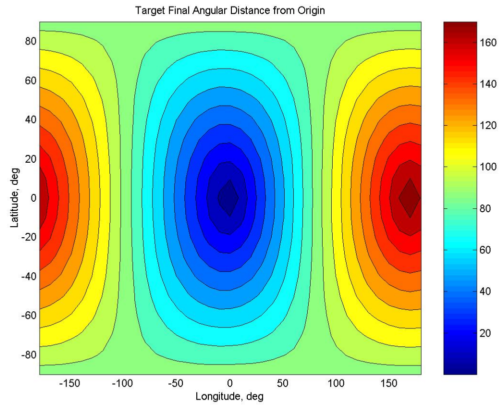

(a) Plot of angular distance between the launch location and the final target location.

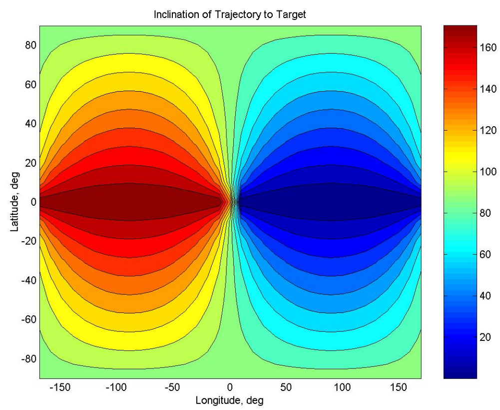

(b) Trajectory's orbital plane inclination angle.

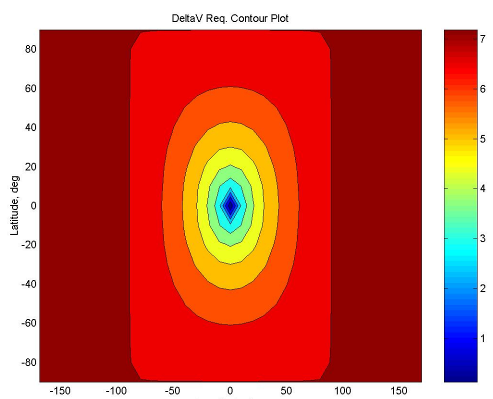

(c) Uncorrected initial inertial velocity plot for launch.

Figure 11: 0º N 0º E s in the 703 point array. Original positions shift in longitude easterly with rotation during the time of flight. Two-body conditions are provided for the $\beta = \infty$ case.

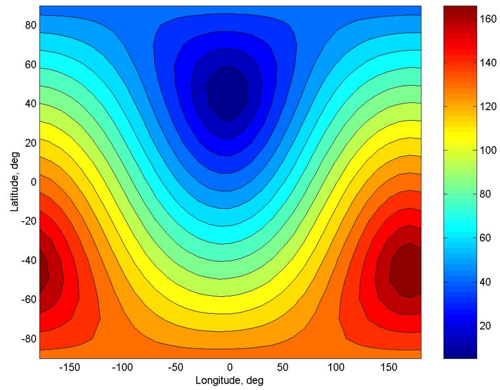

(a) Plot of angular distance between the launch location and the final target location.

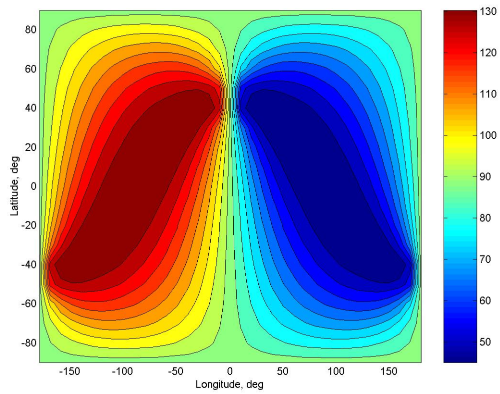

(b) Trajectory's orbital plane inclination angle.

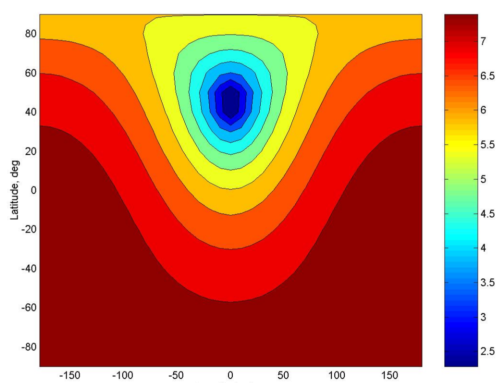

(c) Uncorrected initial inertial velocity plot for launch.

Figure 12: Plot of trends for launch location 45^o N 0^o E and the final target locations in the 703 point array. Original positions shift in longitude easterly with rotation during the time of flight. Two-body conditions are provided for the $\beta = \infty$ case.

Error is seen to be symmetrical across the equator as we should expect for an equatorial launch case. Also, error at the poles is virtually zero since targets located precisely at the poles do not rotate. Values from the simulation indicate error on the order of 1×10^{-6} km are accounted. Internal storage of values throughout the numerical integration process appears to be the cause of this discrepancy, but remain virtually zero for the purposes of any missile targeting application. We also wish to examine the intrinsic properties of the orbit and inertial launch velocity conditions for the two-body case. Figures 11(b) and 11(c) We make special note that the inertial conditions are reviewed since missiles can take advantage of the rotation of Earth for eastward launches and similarly are penalized by the eastward velocity of the Earth when launching west.

We also examine the case for launch location of 45° N 0° E. We notice here that the angular range will increase diagonally and thus the two-body solution's error due to rotation will increase in these regions. Figure 10 shows the southward trend of error as the launch location is shifted northward. We also note the change in the contour to bulge towards the prime meridian. This trend continues with increasing latitude of the launch site.

We examine the relationship of angular distance, two-body projectile inclination, and inertial initial velocity for the trajectories formed for the 45° N launch case in Figures 10-12(c). Here we discover the inclination of the resultant suborbital trajectories correlate to the launch latitude. We note that the minimum inclination is the same as the launch latitude and the maximum inclination is the retrograde trajectory its counterpart. We also note that there are regions where numerous angles converge at 180° of longitude. We note that we have sharp changes at these locations and this could result in issues for convergent solutions.

8.5.2 External Analytical STM Method for Rotation

The external analytical STM method was utilized in order to create the velocity correction necessary to hit the moving target. Recall, that the external definition means that we compute the STM only once before the iteration loop. Figure 13(a) depicts the number of iterations required across the 703 point grid array.

The iteration contour map includes the colorbar legend denoting increasing iterations. As shown, the regions between -150° W and 150° E have a difficult time converging. To understand why there is such a difficulty the angular distance between the origin and the target site following rotation is analyzed.

We review the angular range of the region where solutions fail to converge (10+ iterations) and determine that these targets are near 180°. However due to the nature of failure modes, numerous discontinuities are introduced into the region of failure. Thus to better to explain the region of failure to converge we look to the plot of trajectory inclination.

For the minimum energy solution for 180°, the trajectory runs precisely along the

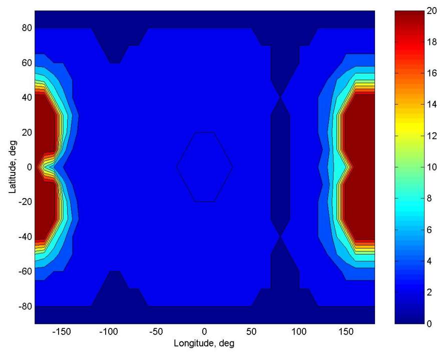

(a) Iteration contour plot analytical method.

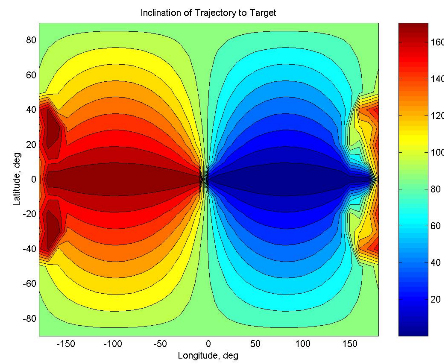

(b) Inclination contour plot analytical method.

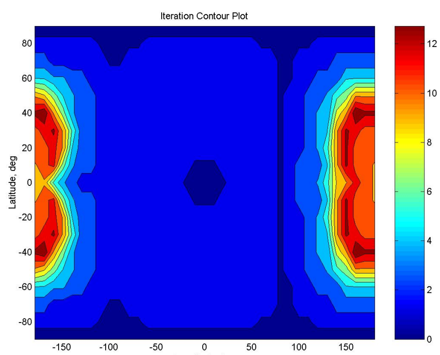

(c) Iteration contour plot numerical method.

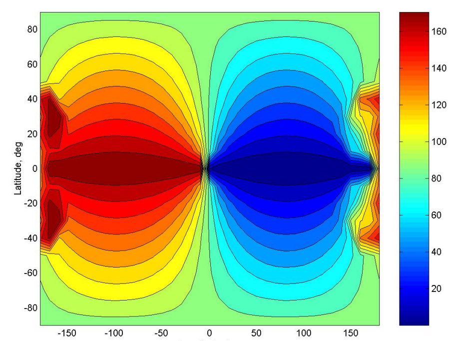

(d) Inclination contour plot numerical method.

Figure 13: launch location 0^o N 0^o E for solutions using the Analytic STM method for the 703 point target array $\beta = \infty$.

surface of the planetary body, or otherwise the apogee altitude is 0 km above the surface. Thus solutions would be difficult to formulate using the minimum energy assumption for this angular range. Figure 13(b) depicts a transitional boundary where the path switches from posigrade (eastward) to retrograde (westward) trajectories. This boundary seems to well define the region where iterations increase and has the most direct correlation to the increase in required iterations.

As indicated in Figure 13(b), the band of trajectories using 0° inclination is depicted as a narrow gap approaching 160° E. This correlates to the narrow region of convergence that penetrates the iteration contour plot in the same area. Similarly a region exists for 180° of inclination on the western portion of the grid. The solution seems to break down earlier on the eastern side of the plot than the western side. This may be attributed to the fact that the eastern portion of the map has a higher angular displacement of the solution. Launching eastward is a more difficult task to catch up to a surface point near 180° than if launching westward. Here the iteration method is switching between launching eastward and westward and having difficulty resolving a solution since large velocity changes are required to completely change direction and thus a large number of iterations.

8.5.3 External Numerical STM Method for Rotation

The external numerical STM method is then examined for the rotation only case to determine its effectiveness. We determine that the numerical method produces very similar plots to the analytic method, however, they differ in important ways. Shown in Figure 13(c), we see that some escape cases are not present. While, the general trend to increase the number of required iterations does seem similar, several regions converge using the external numerical STM where the external analytic solution could not. On average the pure numerical STM requires nearly twice as much computing time to complete the simulation than does the pure external analytic STM method at this ballistic coefficient. We do discover from the examination of resultant trajectory inclination that we see very similar plots between the external analytic method and the external numerical method as shown in Figure 13(d).

8.6 Atmospheric Effects

The addition of atmospheric effects began by defining the ballistic coefficient for values of less than ∞. 3 cases are reviewed for missiles of various order of magnitude $\beta = 2 \times 10^{12}$, 2×10^{9}, and 200×10^{6} kg/km^2. Our results are summarized in tabular form for the launch location of 0° N 0° E. We expect trends to continue as indicated by the rotation only cases for increasing launch latitude and therefore only examine this case in great detail.

8.6.1 Uncorrected Two-Body Solution for $\beta = 2 \times 10^{12}$

The first case examined is $2{\times}10^{12}\frac{\text{kg}}{\text{km}^2}$. This value is very large for any vehicle, but is a good introduction to the effects of drag, and provides a check if drag in the model that is working correctly. Shown in Figure 9(b) is the uncorrected velocity as derived from the two-body non-rotating solution.

8.6.2 Uncorrected Two-Body Solution for $\beta = 2 \times 10^{9}$

Next the $\beta = 2 \times 10^9$ case is explored a realistic value for ballistic missiles. Figure 9(c) shows the uncorrected error on the non-rotating two body solution. Here we notice that error increases significantly and note the change in scale on the colorbar from the previous example.

8.6.3 Uncorrected Two-Body Solution for $\beta = 200 \times 10^{6}$

Figure 9(d) shows the uncorrected error resultant from the two-body initial guess. Error approaches 2000 km for the cases near 150^o E and W longitude while error for the region of study is near 1200 km. Values of this ballistic coefficient are actually too low as they slow down too much in the atmosphere and would be easily intercepted.

8.7 Summary of Methods

For the two sets of target arrays and various ballistic coefficients tested the results are presented for the 4 methods discussed for a launch location of 0^o N 0^o E. Subsequent results from alternative launch locations appear to follow the trends indicated by the test results in Table 8.7.

We see that the analytical method proves to maintain its computational ability at resolving the targets in the array throughout the differences of the array. We can hypothesize that this works by simulating a different average rate that the target is moving (i.e. the rotation of the Earth). Since the method already seems to account for these effects of different rotational speeds at various latitudes, the relatively minimal addition of flight time which causes additional rotation of the Earth can be accounted for in this method.

The numerical method seems to be more computationally robust at arriving at solutions where the analytical solution fails. We should expect this as numerical methods are not limited by analytical conditions. However, the initial guess still creates a unique problem that will need to be addressed in future work. The numerical method in particular did not converge upon solutions for the $\beta = 200 \times 10^6$ case as the direction detection protocols introduced during the modelling of drag appear to have broken down inside the variable step size integration technique.

β kg/km^2	STM Method	Target Array	Convergence Quality	Remarks
∞	EA	No Drag	Conditionally Good	Failure at $\approx$ 180 deg.
...	IA	...	Conditionally Good	Failure at $\approx$ 180 deg.
...	EN	...	Conditionally Excellent	Remote Failures at $\approx$ 180 deg.
...	IN	...	Conditionally Excellent	Remote Failures at $\approx$ 180 deg.
2×10^{12}	EA	Drag	Excellent	No Failures
...	IA	...	Excellent	No Failures
...	EN	...	Excellent	No Failures
...	IN	...	Excellent	No Failures
2×10^{9}	EA	Drag	Excellent	No Failures
...	IA	...	Excellent	No Failures
...	EN	...	Conditionally Excellent	Remote Failure
...	IN	...	Excellent	No Failures
200×10^{6}	EA	Drag	Excellent	No Failures
...	IA	...	Excellent	No Failures
...	EN	...	Computationally Rigorous	DNF
...	IN	...	Computationally Rigorous	DNF

External (E), Internal (I), Analytic (A), Numerical (N), Did not finish (DNF)

9 Conclusions and Future Work

We find that both the numerical and analytical methods have their merits. The numerical method is robust in some cases when the analytical solution breaks down such as the 180 degree exception cases for high values of ballistic coefficient. Internal methods are more computationally expensive than are external methods that are only implemented once however generally reduce the magnitude of error faster. The analytic method is calculated with the same speed at every iteration for all values of β, while the numerical method is slowed significantly as β decreases. The numerical method is computationally expensive and induces numerical failures in the simulation at the lowest chosen β. We can hypothesize that the variable step size performed by the ODE45 numerical integrator is creating these problems.

To alleviate these errors a 2 step approach is proposed for future work. The first step is to numerically integrate to exactly 400 kft (or 122km where the atmosphere is first introduced on the rising portion of the trajectory). We can do this using the event detection protocol similar to that used for detecting an impact on the ground. Once this event is triggered, you can stop the simulation and use the final state(position, velocity) at 400kft for continued simulation using drag on all the time. This integration scheme would still employ the ground strike event detection method. By doing this we eliminate the direction and altitude checks within the drag program which create difficulties with a variable step size integrator. Using this method should also allow us to readily compute solutions with lift and additional atmospheric factors.

We also note that the analytic method has proven especially useful for accounting for drag in this problem. This seems to be due to the fact that the additional flight time required to proceed around the spherical body is not nearly as significant as are effects of the rotation. Since the projectile's studied still had high values of ballistic coefficient, they were not slowed by a large fraction of their velocity at the interface with the significant atmosphere. For the lowest values of ballistic coefficient studied we found that the additional time of flight was only about 4 minutes or 10% for the longest of trajectories.

In addition to completing analysis of a dense target grid as used for the $\beta = \infty$ case, further research will be conducted in the future to make these methods more robust and fault proof. This includes the piecewise integration scheme outlined above in addition to considering a new initial guess for trajectories nearing 180 degrees of angular range. After utilizing this new initial guess (not the minimum energy solution) we should find that convergence rates will improve. Different numerical integration methods can also be researched in further detail as well as the application of the event detection method used to create the spherical surface constraint. Effects of J_2 will also be examined, though anticipated to be minimal for these relatively short flight times. However, use of various altitudes instead of the spherical Earth model will effect results. Drag modulated and lift modulated re-entry vehicles will also be investigated and modelled in future work to create a flexible dynamics program. Effects of a rigid body may also be introduced in future ballistic problem work to determine accuracy from rotation of the warhead about the length of the projectile. Problems will also require examination of shallow trajectories where the projectile may skip off the atmosphere.

Lastly, in the future the ballistic missile defense problem's other components will require analysis. An array of radar location sites could be introduced into the problem to indicate effective tracking of the ballistic missile. Similarly missile interceptors can be introduced and success rate of intercept based on location can be attained. Thus through increasing fidelity of these models and creation of simulation techniques a multitude of publications can be based on this work.

References

[1] Miele, A., *Theory of Flight Paths*, Vol. 1,, Addison-Wesley Publishing Company, Palo Alto.

[2] Schaub, H. and Junkins, J., *Analytical Mechanics of Space Systems*, AIAA Education Series, Reston, VA, 2003.

[3] Battin, R. H., *An Introduction to the Mathematics and Methods of Astrodynamics*, AIAA Education Series, New York, 1987.

[4] Bate, R. R., Mueller, D. D., and White, J. E., *Fundamentals of Astrodynamics*, Dover Publications Inc., New York, 1971.

[5] McFarland, J. S., "Dynamic Sensitivity Considerations of Non-Lifting Ballistic Re-Entry Vehicles," AIAA Region I - NE and MA, College Park, Maryland, April 11-13 2003.

[6] Loh, W. H. T., "Dynamics and Thermodynamics of Re-Entry," *Journal of the Aerospace Sciences*, Vol. 27, 1960, pp. 748–762.

[7] Regan, F. J. and Anandakrishnan, S. M., *Dynamics of Atmospheric Re-Entry*, American Institute of Aeronautics and Astronautics (AIAA), Washington, DC, 1993.

[8] Wertz, J. and Larson, W., editors, *Space Mission Analysis and Design*, Space Technologies Series, Microcosm Press and Kluwer Academic Publishers.

[9] Larson, W. and Pranke, L. K., editors, *Human Space Mission Analysis and Design*, Space Technologies Series.